Electrical Tuning of the MoO_x/Ag Hybrids and Investigation on Their *SERS* Performance

Yinghao Xu, Kui Lai, Chenjie Gu, Tao Jiang*, Xiang Shen, Shuwen Zeng*, Aaron Ho-Pui Ho, Diing Shenp Ang, and Jun Zhou*

Y. H. Xu, K. Lai, Assoc Prof. C. J. Gu, Assoc Prof. T. Jiang, Prof. X. Shen, and Prof. J. Zhou
Ningbo University, No. 818 Fenghua Road, 315211, China
E-mail: guchenjie@nbu.edu.cn; Jiangtao@nbu.edu.cn

Dr. S. W. Zeng
XLIM Research Institute, CNRS/University of Limoges, Avenue Albert Thomas, 87060 Limoges, France
E-mail: shuwen.zeng@unilim.fr

Prof. Aaron H.P. Ho
Department of Electronic Engineering, The Chinese University of Hong Kong, Shatin, NT, Hong Kong SAR

Assoc Prof. D. S. Ang
School of Electrical and Electronic Engineering, Nanyang Technological University, 50 Nanyang Avenue 639798, Singapore

Keywords: surface enhanced Raman scattering; electrical programing; molybdenum oxide/Ag NPs hybrids; electromagnetic enhancement

Surface enhanced Raman scattering (*SERS*) technology has become a cutting-edge analytical tool for molecule detections. Nowadays, attractive *SERS* performance has been achieved on noble metal nanostructures, however these substrates usually suffer from the difficulties of direct adjusting the physical structures to achieve tunable *SERS* performance. Meanwhile, studies on the semiconductor oxides reveal that attractive *SERS* performance can be obtained on them, but strategies of engineering material property for *SERS* performance improvement still pose as a challenge. Here, an electrically programmable *SERS* substrate is prepared by depositing the hydrothermal synthesized MoO_x/Ag hybrids within the electrodes as *SERS* active region. In the experiment, electrical field is applied on the electrodes to regulate the Ag^+ ion migration and redeposition in the MoO_x solid electrolyte. Through adjusting the leakage current level, the size of Ag NPs in the

MoO_x/Ag hybrids is electrically controlled. The *SERS* performance of the substrate is evaluated by using the rhodamine 6G as the Raman reporter. Results evidence that Raman enhancement factor of 1.13×10^5, 4.75×10^5 and 1.04×10^6 can be obtained by programing the leakage current level to 10^{-7}, 10^{-5} and 10^{-3} A, respectively. And maximum detection limit of 10^{-8} M is achieved on the 10^{-3} A substrate.

Surface enhanced Raman scattering (*SERS*) technology is renowned for the merits of non-destructive analysis, ultrahigh sensitivity and molecular fingerprint specificity. It has gained extensive research interests for the potential applications in analytical chemistry, biochemical detection and food safety etc.[1] Today, the mechanism understanding of the *SERS* phenomenon is classified as electromagnetic mechanism (*EM*) and chemical mechanism (*CM*).[2] For the *EM*, the incident light interacts with the noble metals and induces surface plasmon resonances (*SPRs*). These *SPRs* bring significantly enhanced surface electromagnetic fields, which produces 10^6 or higher Raman intensity enhancement.[3] On the other hand, the *CM* is always triggered by the photo induced charge transfer (*PICT*) between the adsorbed molecules and the *SERS* substrate with the help of defect levels in the oxides.[4] As a result, the molecular polarizability is significantly amplified, producing attractive *SERS* enhancement.

Up to date, noble metals (Au or Ag, etc.) in the form of nanoparticles or nanostructures are used as *SERS* substrates for the purpose of generating strong *SPRs* to gain admirable performance.[5] And methods like chemical synthesis or semiconductor fabrication techniques are widely used to prepare these nanoparticles or nanostructures. For example, Hiramatsu et al. reported a versatile and productive method of preparing nearly mono-dispersed gold or silver nanoparticles with adjustable sizes.[6] By modifying the chemical ratio of the tetrachloroauric acid/silver acetate and oleylamineoleylamin, large-scale synthesis of gold (6-21 nm) and silver (8-23 nm) nanoparticles with the relatively low polydispersities of 6.9% could be achieved. Similarly, Lv et al. reported the preparation of gold stars with the core sizes from 26 nm to 50 nm and branches from 7 nm to 10 nm by change the mole ratio of tetrachloroauric acid ($HAuCl_4$), ascorbic acid (AA) and 4-(2-Hydroxyethyl)-1-piperazinyl]-ethanesulfonic acid (HEPES), and each morphology showed distinctive *SERS* performance, which was ascribed to the change of the localized *SPRs* frequency.[7] In the meanwhile, semiconductor fabrication processes of electron-beam-lithography patterning, metal sputtering deposition, selective etching and annealing are alternative ways used to fabricate

nanostructures for *SERS* application.[8] However, these approaches always require complex experiment designs and accurate parameter control. Furthermore, the above prepared noble metal nanostructures also hit the obstacle of flexible adjusting the physical structures to achieve tunable *SERS* performance for the detections of molecules with different *SERS* activities.

Oxide semiconductors have been widely investigated for their admirable light-mater interaction capabilities and tunable optical property.[9] Recently, the out breaking of the material synthesizing and defect engineering methods has brought intensive researches on the oxide semiconductors as the *SERS* substrate.[10] In the literature, inspiring results have demonstrated that oxide materials like titanium oxides (TiO_2), cuprous oxides (Cu_2O), zinc oxides (ZnO), reduced graphene oxides (rGO), tungsten oxides (WO_{3-x}) and molybdenum oxides (MoO_x) show exceptional *SERS* characteristics, which are ascribed to the defect level assisted *PICT* and enhancing the *CM*.[11] Meanwhile, in order to prepare oxide semiconductors with prominent *SERS* activities, diverse oxide defect engineering strategies have been developed. For example, reductant like $NaBH_4$, dopamine, ascorbic acid (AA), polyethylene glycol (PEG), glucose, ethanol etc. are experimentally used to tune the oxygen vacancy density in the chemical synthesized oxide.[12] In addition, methods like dopant intercalation, dopant implantation, light irradiation, crystal phase manipulating and electrochemical deposition are also extensively used to modify the material properties, introducing abundant defect levels in the band structure of oxides and promoting the *PICT*.[13] To date, despite the fact that the existing strategies give the widely tunable defect density and consequently the localized surface plasmon resonance (*LSPR*) properties in the oxides, most of the semiconductor oxides still suffer low *SERS* enhancement capability. Lately, hybrid *SERS* substrates prepared by combining both noble-metal materials and oxides have attracted increasing attentions. The *SERS* performances of oxide/noble metal hybrid structures, for example TiO_2-Au, TiO_2-Ag, MoO_x-Au, graphene oxide/Ag, ZnO/Ag and MoO_x-Ag hybrid substrates have been evaluated in the research. Relying on the synergetic effects of *EM* and *CM*, attractive *SERS* improved performance has been achieved.[14] Nevertheless,

it should be mentioned that preparation of metal-oxide/noble metal hybrids always involves multi-steps of chemical synthesis or extra fabrication process. Additionally, similar as the noble metal nanostructures, most of these oxide/noble metal hybrids also confront the disadvantages of unchangeable structures, which impede the tunability of the material optical characteristics.

Herein, we report an electrically programmable *SERS* substrate prepared by depositing the hydrothermal synthesized MoO_x/Ag hybrids between the Au electrodes with 10-μm space. Then, electrical field is applied between the electrodes to regulate the Ag^+ ion migration and redeposition dynamics in the MoO_x electrolyte. Through adjusting the leakage current level between the electrodes, experimental results demonstrate that the size of Ag NPs in the MoO_x/Ag hybrids could be precisely tuned. Moreover, the *SERS* performance of the prepared substrate is evaluated by using the rhodamine 6G (*R6G*) as the Raman reporter. The measured *SERS* spectra evidence that the detection capability of the substrate can be promoted when the leakage current increases, and with the continuous raising of the leakage current level to 10^{-3} A, maximum Raman enhancement factor of 1.04×10^6 and detection limit of 10^{-8} M can be achieved. In all, this novel *SERS* substrate provides an attractive way of preparing a dynamically tunable *SERS* substrate for high sensitivity sensing applications.

MoO_x/Ag hybrids were synthesized by a quick (3 hours) and low temperature (80 ºC) hydrothermal method (see the Material Synthesis in Experimental Section).[12] Scanning electron microscopy detection was first performed. As shown in the **Figure 1(a)** and **(b)**, MoO_x nanorods with the diameter of 250 nm are detected, and sparse Ag NPs randomly anchor on the MoO_x nanorods, indicating that the MoO_x provides good nucleation sites for Ag NPs. Thereafter, transmission electron microscopy (*TEM*) analysis in **Figure 1(c)** discerns that the average size of the synthesized Ag NPs is about 7.2 nm, while the high resolution TEM (*HRTEM*) image (inset of Figure 1(c)) reveals that the lattice space of the synthesized MoO_x nanorode is 3.518 Å, which corresponds to the (200) face of the monoclinic MoO_3. And the lattice space of the Ag NP is 1.139

Å, which reflects the (311) face of Ag metal. Selective area electron diffraction (*SEAD*) analysis was also performed on the hybrids. The obtained diffraction pattern shown in **Figure 1(d)** reveals that the (100), (101) and (200) face of the monoclinic crystal phase. Finally, the electron dispersion spectra (*EDS*) element mapping in the **Figure 1(e)** further confirms that the MoO_x nanorods surface is covered by Ag NPs

The optical properties of the MoO_x/Ag hybrids were investigated as well. The *UV-vis* absorption spectra of the MoO_x/Ag hybrids and pure MoO_x are shown in the **Figure 2(a)**. The spectra measured on MoO_x/Ag hybrids display a strong absorption peak near 210 nm, which is induced by the light absorption of the tetrahedral MoO_x. In the meanwhile, two weak and relatively broad absorption humps appear near 236 and 275 nm (band 1 and 2), which are contributed by the Mo^{6+} in an octahedral structure. While the fourth weak absorption peak near 330 nm is ascribed to be the interaction between the Ag NPs and incident light (band 3). On the other hand, the *UV-vis* absorption spectra measured on MoO_x only show the band gap absorption edge (wavelength < 350 nm), and the absorption induced by the defects at the long wavelength (wavelength > 500 nm) is very weak, indicating the MoO_x prepared in this work is defect deficiency.[15] The Raman spectra of the MoO_x/Ag hybrids were collected and shown in **Figure 2(b)**. It can be observed that the spectra are comprised by complex Raman vibrational modes. The characteristic peaks at 366 cm^{-1} can be assigned to the vibrational modes of σ (Mo=O), and peaks at 596 and 63 cm^{-1} are attributed to the γ (Mo-O-Ag) vibrational mode, indicating the formation of the Ag-O bond during the reduction process. In addition, the peak at 870 cm^{-1} is assigned to *v* (Mo-O-Mo) vibrational mode, whereas peaks at 910 and 938 cm^{-1} are ascribed to the *v* (Mo=O) vibrational modes.[16]

To realize the electrical tuning of the MoO_x/Ag hybrids, in the subsequent steps, the MoO_x/Ag hybrids (wt%: 2.5%) were dissolved in H_2O and ethanol (5:3) mixed solution again, sonicated for 10 min, and then spin coated on the Si wafer with prefabricated 100-nm thickness of paired Au electrodes. The prepared substrate was annealed at 80 °C for 0.5 h in the air to improve the

adhesion. **Figure 3(a)-(c)** shows the optical image, schematic structure and SEM image of the prepared *SERS* substrate. It can be found that the spin-coated MoO_x/Ag hybrids remain the nanorods morphology and form thin film on the wafer surface with 92-nm physical thickness (**Figure 3(d)**). More specifically, the MoO_x/Ag hybrids in the space between the Au electrodes with the dimension of 10×10 μm^2 composes the *SERS* active region, while the two electrodes are used to electrically program the active region.

Electrical tuning of the MoO_x/Ag hybrids in our work was conducted by using a Keithley 4200-SCS semiconductor parameter analyzer. As an electro-active material, the anodic dissolution rate of the silver metal under the electrical field can reach 35.6 $nm \cdot s^{-1}$.[17] In the experiment, when the electrical bias was applied on the electrodes, the Ag anodically dissolved and Ag^+ ions migrated along the electrical field towards the cathode in the MoO_x oxide electrolyte. During the migration process, the Ag^+ ions were reduced when they met the electrons from the cathodes, and redeposited near the cathodes side again.[18] Relying on the above electro-migration mechanism, the dissolution rate of Ag^+ ions were controlled through adjusting the current level between the electrodes during the programing period, and consequently the size of the redeposited Ag NPs were regulated within the oxide electrolyte. Therefore, in our experiment, the current level through the *SERS* active region was controlled by setting the current compliance during the voltage sweep on the two electrodes (**Figure 4(a)**). Typically, three similar *SERS* substrates with the designated leakage current level (10^{-7}, 10^{-5} and 10^{-3} A) were programmed, respectively. At this stage, it was worth noting that, for the purpose of preventing catastrophic breakdown of the MoO_x/Ag hybrids when the voltage exceeded a certain threshold voltage (>100 V), our voltage sweeps were carried out in multi-steps. In the first step, when the MoO_x/Ag hybrids was in the pristine state, the current compliance was set to 10^{-7} A. When the sweep voltage climbed, the leakage current simultaneously increased until it reached the first compliance of 10^{-7} A, then the sweep voltage was stopped. Thereafter, for the device needed to be programmed to higher leakage current, the current compliance was tuned to 10^{-}

^{5} A and 10^{-3} A, respectively, and the voltage sweep was applied again until the leakage current finally reached the specific level. At this moment, it could be found from the I-V curve in Figure 4(a) that, below the threshold voltage, all three devices own relatively low leakage current ($<1\times10^{-10}$ A@1V). This indicates that, although Ag NPs are stationed on the MoO_x nanorods, the density of the Ag NPs is relatively low, and thus they are not connected with each other to form the current path. However, only after the voltage sweep, the migration of Ag^+ ions and gradual increase of the Ag NPs size forms the current path, resulting in the rising of the device leakage current.

The *SERS* performance was evaluated by using the rhodamine 6G (*R6G*) as the probe molecules. During the measurement, a 532-nm semiconductor laser was used as the excitation source, and the spot diameter of the laser on the substrate was 12.5 um (100× objective lens), which could cover the *SERS* active area. The Raman spectra were collected under a laser power of 1 mW with an integration time of 10 s. The measured Raman spectra were shown in **Figure 4(b)**. It can be found that no detectable Raman peak can be observed on the silicon substrate when the concentration of *R6G* is 10^{-4} M. On the other hand, relatively faint Raman peaks originate from *R6G* were observed on the pristine MoO_x substrate and pristine MoO_x/Ag hybrids device, which can be ascribed to the weak Raman signal enhancement of these two substrates (see **Figure S1** in the Supporting Information). Furthermore, when the leakage current increase to 10^{-3} A, the fingerprint peaks of *R6G* are enhanced remarkably, indicating the *SERS* performance of the MoO_x/Ag hybrids is improved through the electrical programing. In detail, prominent Raman peaks of *R6G* at 609, 769, 1193, 1355, 1471, 1538, 1605 and 1646 cm^{-1} are observed on the collected *SERS* spectra. The peaks located at 609 cm^{-1} is due to the C-C-C ring in-plane bending, and 769 cm^{-1} is assigned to out-of-plane bending of the C-H atom on the xanthene's skeleton. Moreover, peak at 1193 cm^{-1} arises from the C-H in-plane bending. And the peaks from 1355 to 1646 cm^{-1} belong to aromatic C-C stretching vibration modes. In addition to that, the Raman signals intensities on substrates with the 10^{-5} A and 10^{-7} A programmed leakage current were also collected and shown in Figure 4(b). Impressively, the

measured Raman intensity decreases with the reducing of the leakage, revealing that the change of MoO_x/Ag hybrids *SERS* property is closely related to the leakage level and the Raman enhancement capability of the substrate can be electrically programmed by fine control of the voltage sweep. The enhancement factors (EFs) of the three substrates with 10^{-7}, 10^{-5} and 10^{-3} A leakage current are calculated by integrating the Raman peak at 1355 cm^{-1} (see the Supporting Information). Through the calculation, Efs of 1.13×10^5 (10^{-7} A), 4.76×10^5 (10^{-5} A) and 1.04×10^6 (10^{-3} A) are achieved for the respective leakage current level, which further verifies the tunable *SERS* performance (**Figure 4(c)**). The detection limit of the substrate with 10^{-3} A is also accessed by detecting the *R6G* solutions with different concentrations. It shows in **Figure 4(d)** that the intensities of the characteristic peaks coincidentally drop with the decrease of the *R6G* concentration, and the minimum detectable concentration of 10^{-8} M can be achieved when the substrate leakage is 10^{-3} A.

In the end, to explore the physical mechanism of the improved *SERS* performance of the MoO_x/Ag hybrids after electrical programming, the optical and SEM image were first investigated and shown in **Figure 5(a)** and **(b)**. It can be observed in the optical image that discernible change of the MoO_x/Ag hybrids happens near the cathodes. In the meanwhile, from the SEM detection on the electrically programmed substrate (Figure 5(b)), it further illustrates that the size of Ag NPs (average size: 38.97 nm) significantly grows up as compared to that (average size: 7.25 nm) in the pristine state, which can be ascribed to the Ag^+ ion electro-deposition on the initial Ag NPs during the voltage sweep step. Moreover, it also can be observed on the SEM image that the MoO_x changes from monoclinic phase (nanorods) to orthorhombic phase (nanoflakes), resulting from the thermal effect during the programing phase.[19] On this basis, it is observed that Ag NPs and MoO_x forms more robust heterojunction after electrical programing, however, band edge alignment between Ag NPs and MoO_x reveals that they form ohmic contact kind of heterojunction, resulting in little help on promoting the charge transfer (see **Figure S2** in the see the Supporting Information).[20] In the meanwhile, as shown in the **Figure S1**, the chemical enhancement from the

pure MoO_x is also insignificant when compared to the total *SERS* enhancement, thus it can be inferred that *SERS* enhancement of the of the MoO_x/Ag NPs hybrids is main contributed by the EM from Ag NPs. Therefore, finite-difference time-domain (FDTD) simulation is performed to investigate the Ag NPs' surface electromagnetic field. The MoO_x/Ag hybrids before and after electrical programing were modeled based on the SEM detection images (see **Figure S3** in the Supporting Information), and the surface electromagnetic fields were extracted. As it is shown in **Figure 5(c)** and **(d)** that LSPR are generated on both MoO_x/Ag hybrids under the light irradiation. However, it also can be clearly found that much stronger surface electromagnetic field exists on the Ag NPs with larger size compared to that on the pristine Ag NPs with relatively smaller size, which consequently boosts the *SERS* performance significantly.

To summarize, an electrical programmable *SERS* substrate prepared by the MoO_x/Ag hybrids is demonstrated. Through controlling the leakage current level, the size of Ag NPs in the MoO_x/Ag hybrids can be precisely controlled. The *SERS* performance with different programmed leakage levels is evaluated by using the *R6G* as the Raman reporter. Experimental results show that tunable Raman enhancement factor of 1.13×10^5 (10^{-7} A), 4.75×10^5 (10^{-5} A) and 1.04×10^6 (10^{-3} A) can be obtained. And maximum detection limit of 10^{-8} M can be achieved on the 10^{-3} A substrate. In the end, physical simulation reveals that the increase of Ag NPs size after electrical programming shifts the LSPR frequency towards the 532-nm laser excitation source, which significantly promotes surface electromagnetic field of Ag NPs and enhances the *SERS* performance.

Experimental Section

Materials: Glucose (99%) was purchased from Macklin; ammonium heptamolybdate (AHM, >99%), silver nitrate ($AgNO_3$, 99.8%), ethanol (99.7 %) and nitric acid (HNO_3, wt%: 68%) were purchased from Sinopharm Chemical Reagent Co., Ltd. All chemicals were used without further purification. In all the experiments, deionized water (resistivity of 18.2 MΩ • cm) was used to prepare the solutions.

Material Synthesizing: MoO_x/Ag hybrids were prepared by a low temperature chemical synthesis reaction. Basically, AHM (882.7 mg) was used as molybdenum source and dissolved into deionized water (25 ml), then the mixed solution was stirred slowly (8000 rpm) at 80 °C. Thereafter, glucose solution (20 ml, wt%: 2.57%) was slowly added into the above mixed solution and stirred for 10 minutes. After that, HNO_3 (150 ul, wt%: 68%) was added into the mixed solution. After one-hour reaction, the mixed solution turned dark blue, and then $AgNO_3$ solution (25 ml, wt%: 1.94%) was slowly added to the above solution, and the stirring rate was accelerated to 15000 rpm for two hours. After the reaction was completed, the product was centrifuged, washed with acetonitrile, ethanol and deionized water, respectively, and finally dried in the oven at 80 °C for 8 hours.

Characterization: Voltage sweep and leakage current measurements were performed using a Keithley 4200-SCS semiconductor parameter analyzer system (Tektronix, US). The SEM images of the substrates were acquired by a Hitachi SU-70 system (Hitachi, Japan) under an accelerating voltage of 5 kV. The TEM images were obtained on a JEM-2100F transmission electron microscope (JEOL, Japan). The UV-vis spectra were collected with a spectrometer (TU1901, P-General, Samutprakarn, Thailand). *SERS* measurements were made by a Raman microscope equipped with a spectrometer (QE Pro, Ocean Optics, USA). A 532-nm semiconductor laser was used as the excitation source, and the diameter of the spot size of the laser on the substrate is 12.5 μm (100× objective lens). The Raman spectra were collected under a laser power of 1mW, and an integration time of 10 s.

Supporting Information

Supporting Information is available from the Wiley Online Library or from the author.

Acknowledgements

This research was funded by National Natural Science Funding of China (Grant No. 61704095), the Natural Science Funding of Ningbo (Grant No. 2019A610058) and the K.C. Wong Magna Fund in Ningbo University.

Conflict of Interest

The authors declare no conflict of interest.

Received: ((will be filled in by the editorial staff))
Revised: ((will be filled in by the editorial staff))
Published online: ((will be filled in by the editorial staff))

References

[1] S. Schlücker, *Angew. Chem. Int. Ed.* **2014**, 53, 4756.

[2] a) M. G. Albrecht, J. A. Creighton, *J. Am. Chem. Soc.* **1977**, 99, 5215; b) A. Otto, *J. Raman Spectrosc.* **2005**, 36, 497.

[3] T. Jiang, G. Chen, X. Tian, S. Tang, J. Zhou, Y. Feng, H. Chen, *J. Am. Chem. Soc.* **2018**, 140, 15560.

[4] S. Cong, Y. Yuan, Z. Chen, J. Hou, M. Yang, Y. Su, Y. Zhang, L. Li, Q. Li, F. Geng, Z. Zhao, *Nat. Comm.* **2015**, 6, 7800.

[5] a) M. Grzelczak, J. Pérez-Juste, P. Mulvaney, L. M. Liz-Marzán, *Chem. Soc. Rev.* **2008**, 37, 1783; b) D.-Y. Wu, J.-F. Li, B. Ren, Z.-Q. Tian, *Chem. Soc. Rev.* **2008**, 37, 1025.

[6] a) H. Hiramatsu, F. E. Osterloh, *Chem. Mater.* **2004**, 16, 2509; b) Y. Tian, H. Liu, Y. Chen, C. Zhou, Y. Jiang, C. Gu, T. Jiang, J. Zhou, *Sens Actuators B: Chem* **2019**, 301, 127142(1.

[7] W. Lv, C. Gu, S. Zeng, J. Han, T. Jiang, J. Zhou, *Biosens. Bioelectron* **2018**, 8, 2.

[8] a) D. Lin, Z. Wu, S. Li, W. Zhao, C. Ma, J. Wang, Z. Jiang, Z. Zhong, Y. Zheng, X. Yang, *ACS Nano* **2017**, 11, 1478; b) L. Jiang, X. Liang, T. You, P. Yin, H. Wang, L. Guo, S. Yang, *Spectrochim. Acta A* **2015**, 142, 50; c) L. Feng, K. Wang, P. Li, W. Wang, T. Chen, *New J. Chem.* **2018**; d) J.-F. Li, Y.-J. Zhang, S.-Y. Ding, R. Panneerselvam, Z.-Q. Tian, *Chem. Rev.* **2017**, 117, 5002; e) J. Yu, M. Yang, Z. Li, C. Liu, Y. Wei, C. Zhang, B. Man, F. Lei, *Anal. Chem.* **2020**, 92, 14754.

[9] a) F. Zhou, Z. Zhou, J. Chen, T. H. Choy, J. Wang, N. Zhang, Z. Lin, S. Yu, J. Kang, H. S. P. Wong, Y. Chai, *Nat. Nanotechnol.* **2019**, 14, 776; b) M. M. Y. A. Alsaif, M. R. Field, T. Daeneke, A. F. Chrimes, W. Zhang, B. J. Carey, K. J. Berean, S. Walia, J. van Embden, B. Zhang, K. Latham, K. Kalantar-zadeh, J. Z. Ou, *ACS Appl. Mater. Interfaces* **2016**, 8, 3482; c) M. M. Y. A. Alsaif, A. F.

Chrimes, T. Daeneke, S. Balendhran, D. O. Bellisario, Y. Son, M. R. Field, W. Zhang, H. Nili, E. P. Nguyen, K. Latham, J. van Embden, M. S. Strano, J. Z. Ou, K. Kalantar-zadeh, *Adv. Funct. Mater.* **2016**, 26, 91.

[10] X. Han, W. Ji, B. Zhao, Y. Ozaki, *Nanoscale* **2017**, 9, 4847.

[11] a) L. Yang, M. Gong, X. Jiang, D. Yin, X. Qin, B. Zhao, W. Ruan, *J. Raman Spectrosc.* **2015**, 46, 287; b) Y. Wang, W. Ruan, J. Zhang, B. Yang, W. Xu, B. Zhao, J. R. Lombardi, *J. Raman Spectrosc.* **2009**, 40, 1072; c) J. Lin, Y. Shang, X. Li, J. Yu, X. Wang, L. Guo, *Adv. Mater.* **2017**, 29, 1604797; d) X. Yu, R. Cai, Y. Song, Q. Gao, N. Pan, M. Wu, X. Wang, *RSC Adv.* **2017**, 7, 14959; e) S. Cong, Y. Yuan, Z. Chen, J. Hou, M. Yang, Y. Su, Y. Zhang, L. Li, Q. Li, F. Geng, Z. Zhao, *Nat. Comm.* **2017**, 6, 7800(1; f) X. Zhou, X. Zhao, F. Xie, Z. Jin, X. Song, W. Xie, X. Wang, Z. Tang, *ACS Appl. Mater. Interfaces* **2020**, 3, 5656; g) C. Zhou, L. Sun, F. Zhang, C. Gu, S. Zeng, T. Jiang, X. Shen, D. S. Ang, J. Zhou, *ACS Appl. Mater. Interfaces* **2019**, 11, 34091.

[12] a) G. Song, J. Shen, F. Jiang, R. Hu, W. Li, L. An, R. Zou, Z. Chen, Z. Qin, J. Hu, *ACS Appl. Mater. Interfaces* **2014**, 6, 3915; b) Y. Li, J. Cheng, Y. Liu, P. Liu, W. Cao, T. He, R. Chen, Z. Tang, *J. Phys. Chem. C* **2017**, 121, 5208; c) J. Wang, Y. Yang, H. Li, J. Gao, P. He, L. Bian, F. Dong, Y. He, *Chem. Sci.* **2019**, 10, 6330.

[13] a) B. Y. Zhang, A. Zavabeti, A. F. Chrimes, F. Haque, L. A. O'Dell, H. Khan, N. Syed, R. Datta, Y. Wang, A. S. R. Chesman, T. Daeneke, K. Kalantar-zadeh, J. Z. Ou, *Adv. Funct. Mater.* **2018**, 28, 1706006; b) Y. Zhan, Y. Liu, H. Zu, Y. Guo, S. Wu, H. Yang, Z. Liu, B. Lei, J. Zhuang, X. Zhang, D. Huang, C. Hu, *Nanoscale* **2018**, 10, 5997; c) X. Jiang, K. Song, X. Li, M. Yang, X. Han, L. Yang, B. Zhao, *ChemistrySelect.* **2017**, 2, 3099; d) V. Brasiliense, J. E. Park, Z. Chen, R. P. Van Duyne, G. C. Schatz, *J. Raman Spectrosc.* **2020**.

[14] a) Y. Guo, Z. Zhuang, Z. Liu, W. Fan, H. Zhong, W. Zhang, Y. Ni, Z. Guo, *Appl. Surf. Sci.* **2019**, 480, 1162; b) Z. Niu, C. Zhou, J. Wang, Y. Xu, C. Gu, T. Jiang, S. Zeng, Y. Zhang, D. S. Ang, J. Zhou, *J. Mater. Sci.* **2020**, 55, 8868; c) X. Zhao, C. Liu, J. Yu, Z. Li, L. Liu, C. Li, S. Xu, W. Li, B. Man, C. Zhang, *Nanophotonics* **2020**, 9, 4761; d) S. Kumar, D. K. Lodhi, J. P. Singh, *RSC Adv.* **2016**, 6, 45120; e) X. Liang, X.-J. Zhang, T.-T. You, G.-S. Wang, P.-G. Yin, L. Guo, *CrystEngComm* **2016**, 18, 7805; f) G. Sinha, L. E. Depero, I. Alessandri, *ACS Appl. Mater. Interfaces* **2011**, 3, 2557.

[15] X. Tan, L. Wang, C. Cheng, X. Yan, B. Shen, J. Zhang, *Chem. Commun.* **2016**, 52, 2893.

[16] E. K. Fodjo, D.-W. Li, N. P. Marius, T. Albert, Y.-T. Long, *J. Mater. Chem. A* **2013**, 1, 2558.

[17] a) V. Brusic, G. S. Frankel, J. Roldan, R. Saraf, *J. Electrochem. Soc.* **1995**, 142, 2591; b) M. Suparna, B. Sharda, S. Gauri, M. Soumyo, *Phys. Sci. Rev.* **2019**, 4, 20170082.

[18] H. Taro *Japan Patent EP3018111A1*, **2016**.

[19] L. Lajaunie, F. Boucher, R. Dessapt, P. Moreau, *Phys. Rev. B* **2013**, 88, 115141.

[20] a) Y. Chen, H. Liu, Y. Tian, Y. Du, Y. Ma, S. Zeng, C. Gu, T. Jiang, J. Zhou, *ACS Appl. Mater. Interfaces* **2020**, 12, 14386; b) P. Guha, A. Ghosh, R. Thapa, E. M. Kumar, S. Kirishwaran, R. Singh, P. V. Satyam, *Nanotechnology* **2017**, 28, 415602.

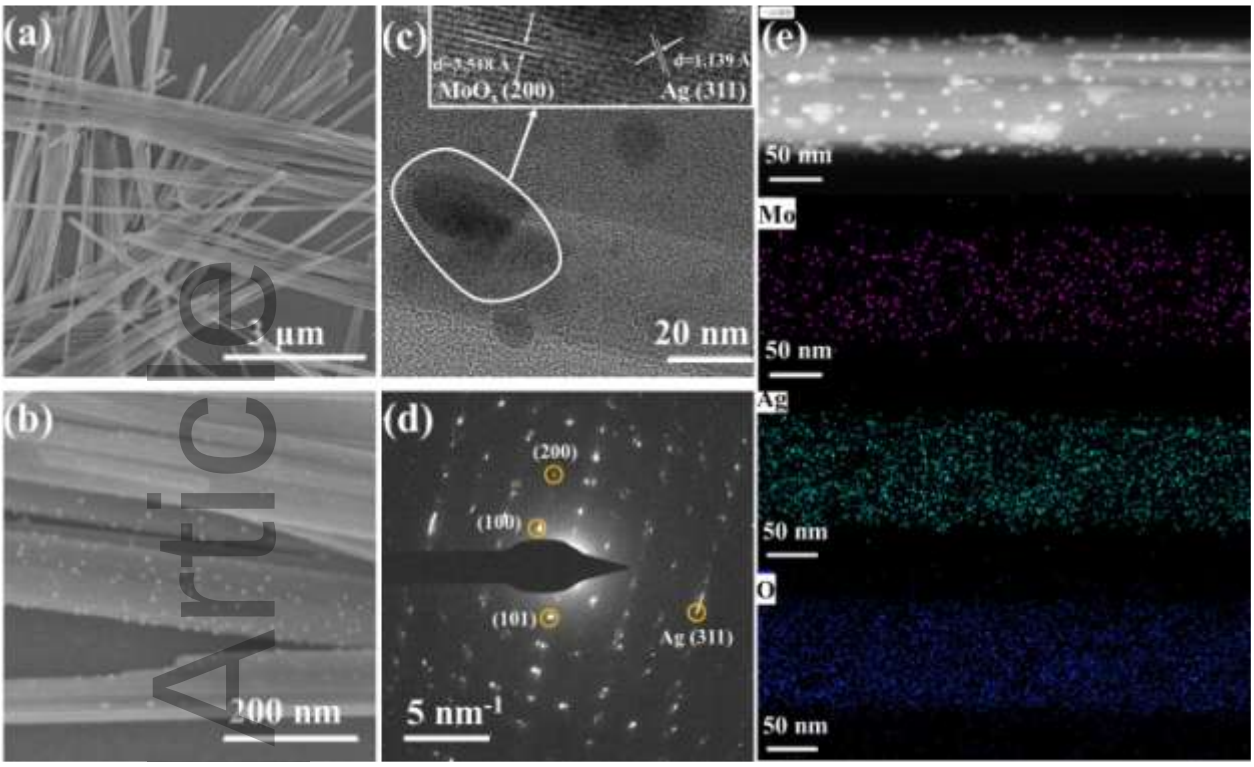

Figure 1. a) and b) The SEM images of the MoO_x/Ag hybrids with different magnifications. c) The TEM image of the MoO_x/Ag hybrids. The inset in (b) shows the lattice space of MoO_x and Ag, respectively. d) The SEAD pattern of the MoO_x/Ag hybrids. e) The EDS mapping images of the Mo, Ag and O element on the MoO_x/Ag hybrids.

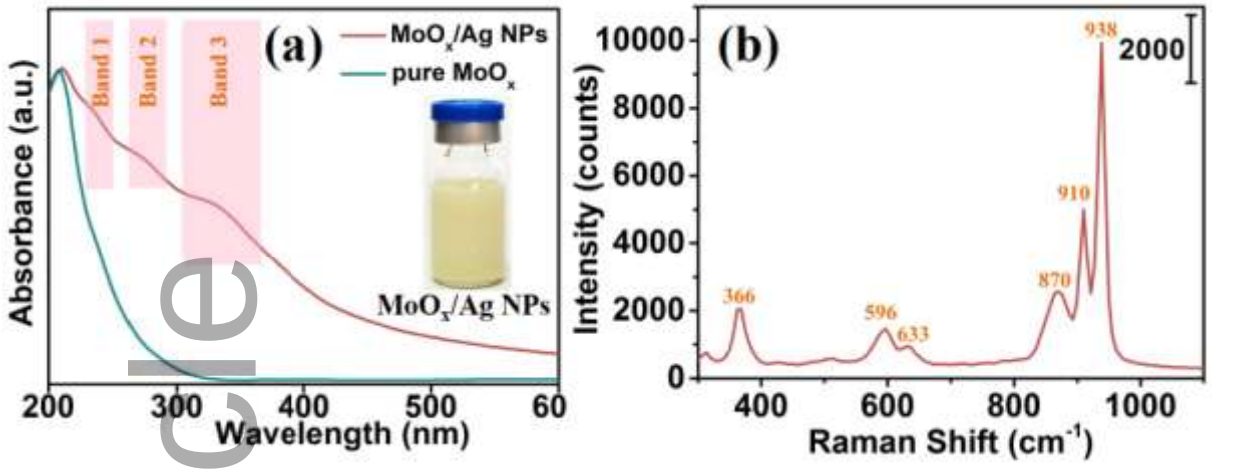

Figure 2. a) The *UV-vis* absorption spectra of the MoO_x/Ag hybrids and pure MoO_x. The inset in (a) shows the optical image of the MoO_x/Ag hybrids solution. b) The Raman spectra of the MoO_x/Ag hybrids.

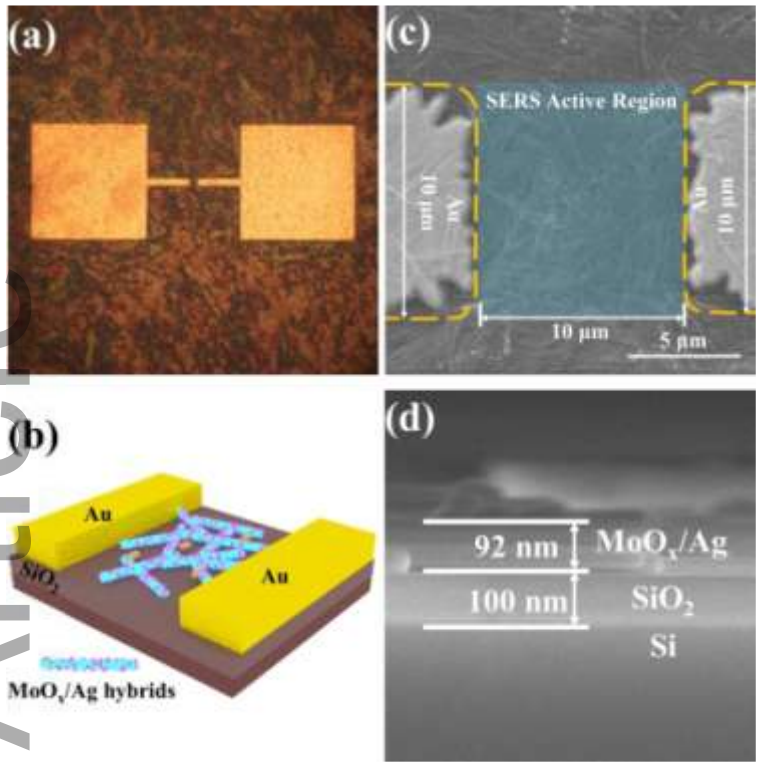

Figure 3. a) The optical image of the pristine substrate. b) The schematic structure of the *SERS* substrate. c) The SEM image of the pristine substrate. d) The SEM cross-section image of the substrate.

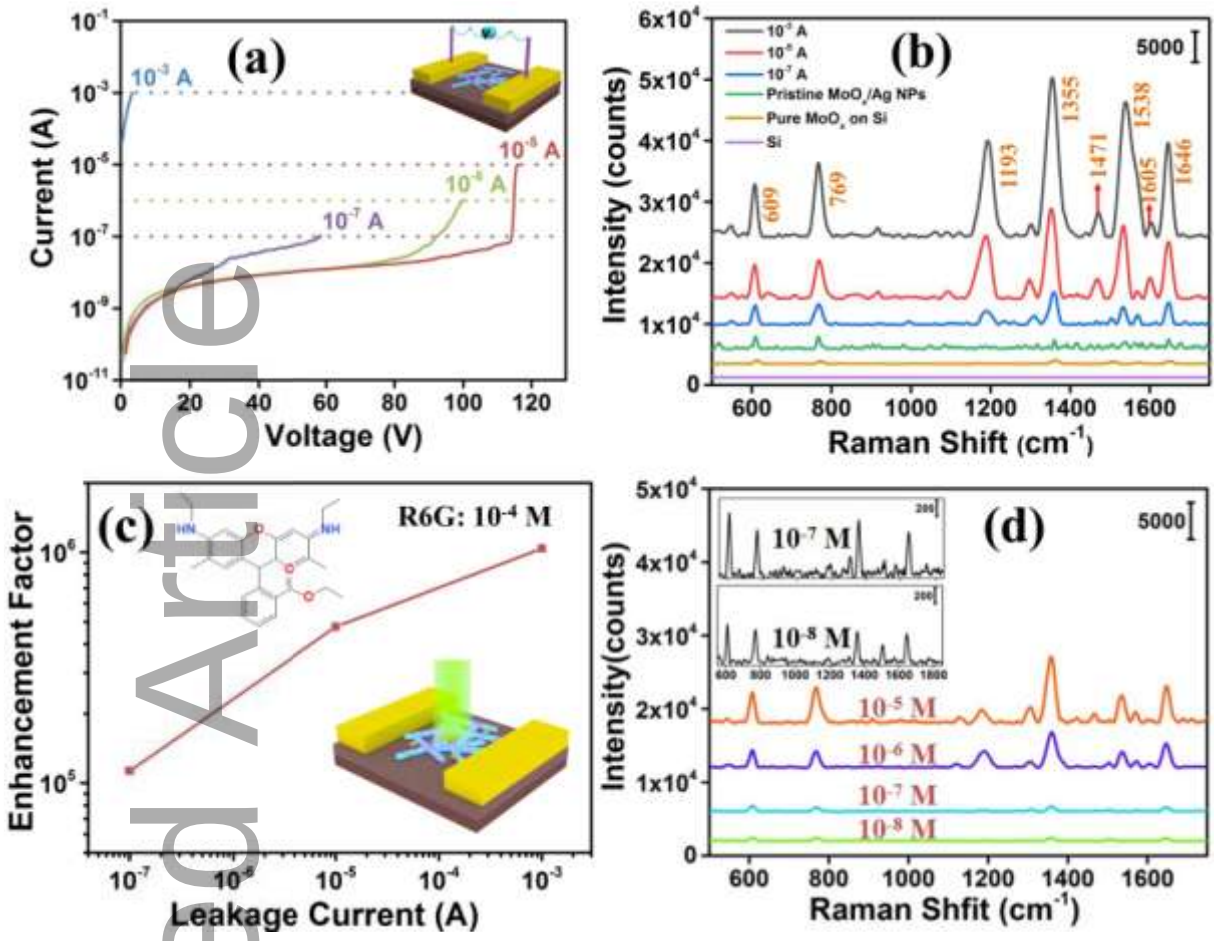

Figure 4. a) The *I-V* curves obtained during the electrical programing. b) The *SERS* spectra measured on different substrates. The concentration of *R6G* is 10^{-4} M. c) The calculated enhancement factor of the substrate with 10^{-7}, 10^{-3} and 10^{-3} A leakage current. d) The detection limited of the substrate with 10^{-3} A leakage current.

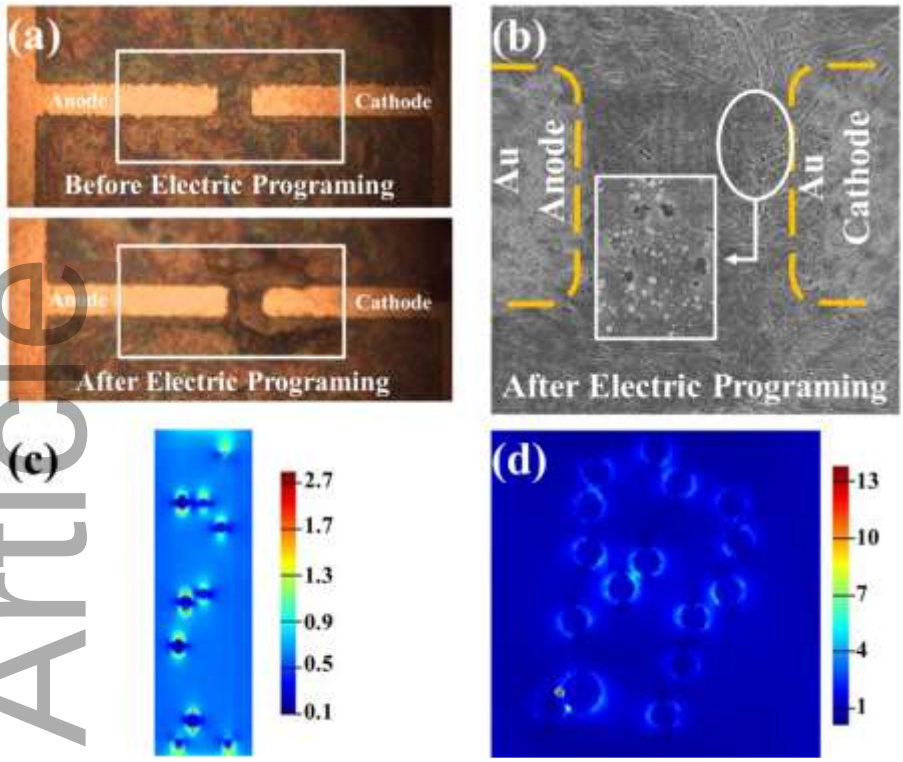

Figure 5. a) The optical images of the *SERS* substrates before and after electrical programming. b) The *SEM* surface image of the *SERS* substrate after electrical programming. c) The simulated surface electromagnetic field of the *SERS* substrate before electrical programming. d) The simulated surface electromagnetic field of the *SERS* substrate after electrical programming.

An electrically programmable *SERS* substrate prepared by depositing the hydrothermal synthesized MoO_x/Ag hybrids is presented. By using the rhodamine 6G as the Raman reporter, tunable *SERS* performance with the Raman enhancement factor of 1.13×10^5, 4.75×10^5 and 1.04×10^6 can be obtained by programing the leakage current level to 10^{-7}, 10^{-5} and 10^{-3} A, respectively.

Keywords: surface enhanced Raman scattering; electrical programing; molybdenum oxide/Ag NP hybrids; electromagnetic enhancement

Electrical Tuning of the MoO_x/Ag Hybrids and Investigation on Their *SERS* Performance

Toc Figure